Adaptive Kalman Procedure for SAR High Resolution Image Reconstruction in the Planning Phase of Land Consolidation

Li Li [a], Ming Luo [b], Chao Zhang [a], Wei Su [a], Yijun Jiang [b], Daoliang Li* [a]
[a] College of Information and Electrical Engineering,
China Agricultural University, Beijing,
P. R. China, 100083
[b] Land Consolidataion Center, the Ministry of Land Resourses
P. R. China, 100035
*Corresponding author: Daoling Li (Prof.) Tel: +86-10-62736717, Email: li_daoliang@yahoo.com

Abstract: -Remote Sensing technologies provide the spatial data/maps and offer great advantages for a land consolidation project. But sometimes in some regions, optics and infrared remote sensing can not work well. SAR (Synthetic aperture radar), an active microwave remote sensing imaging radar, has the unique capabilities of obtaining abundant electromagnetic information from ground objects all day/all night and all weather, and penetrating some special objects and detecting the shapes of ground objects. At this point, SAR can meet the requirement. However, for land consolidation application, high spatial resolution SAR images are required. To increase the spatial resolution of SAR images, this work presents a novel approximate iterative and recurrent approach for image reconstruction, namely adaptive Kalman Filter (KF) procedure. Mathematical models and Kalman equations are derived. The matched filter and Kalman Filter are integrated to enhance the resolution beyond the classical limit. Simulated results demonstrate that the method strongly improves the resolution by using prior knowledge, which is a scientific breakthrough in the case that the traditional pulse compression constrains the improvement of SAR spatial resolution. And it is also shown that it is an optimal method in the sense of mean square error and its computation cost is lower than the traditional Kalman Filter algorithm.

Key-Words: - Land, Agriculture, Synthetic Aperture Radar, Adaptive Kalman Filter, High Resolution, Mean Square Error, Image Reconstruction

1 Introduction

Land consolidation refers to a serial of activities, which deal with improving of productivity and working conditions in rural areas, production of reconstruction plans for rural settlement, and proving of rural life. It has been associated with broader social and economic reforms from the time of its earliest applications in Western Europe [1]. Due to the growing concern about land resource management and the associated decline in land quality in many countries, land consolidation has become one of the most attractive worldwide research topics [2, 3, 4, 5]. Why land consolidation is so important? Because Land consolidation is a tool for improving the effectiveness of land cultivation. A study indicated that land consolidation may improve land productivity and possibly also the total factor productivity if it induced and enhanced technical progress and increased scale economies [6]. Other researchers find that land consolidation can also improve labor productivity [7 , 8]. So land consolidation can not only lead to improvements in agriculture but also promote management of natural resources and rural development.

However, the fulfillment of all those functions more or less depends on supplement of spatial data. There are a variety of manners to collect spatial data. For a sound collection method, speed and ease crucially improve the productivity of a land consolidation. At this point, remote sensing technologies provide the spatial data/maps and offer great advantages for a land consolidation project.

Significant developments in the field of remote sensing, especially in terms of spatial and spectral resolution, have facilitated the manipulation of efficient and precise spatial database. The use of remote sensing high resolution images, mainly from optics and infrared remote sensor such as IKONOS, Quick bird etc., will be extremely feasible in the land projects[9, 10]. Especially in the planning phases, the remote sensing data will have met the requirements of decision makers at various scales from regional to village level. It can also serve a wide range of applications through a centralized database to various government organizations, public undertakings and non-governmental organizations [11].

In the planning stage of a land consolidation work, the following work can easily be done in the required precisions by using remote sensing satellite.

· Determination of present state of project area;

· Land works and classification processes;

· Formation of blocks (water management, drainage and road systems);

· Determination of stationary establishments images.

By using satellite images, they can be completed in half of the time that classical techniques require and the project can cost 35 times cheaper than that the classical techniques cost.

But cloud and rain influence the quality of the optics and infrared imagery greatly. In some regions where clouds usually hide the day, the weather conditions hamper optical image acquisitions. Furthermore, when there are a lot of atmospheric particles, the sunlight will be scattered intensely and the images will be fogged. Under these conditions, the imagery is difficult to unscramble.

Synthetic aperture radar (SAR) remote sensing, with its advantages of all-weather coverage, all day/night acquisitions, cloud penetration, and signal independence of the solar illumination angle, can be applied to land cover classification and land consolidation, especially in some regions where optics and infrared remote sensing do not work well. Its unique capabilities greatly propel and improve the SAR applications to many fields[12, 13, 14], including land cover classification and land consolidation.

Nevertheless there are some uncertain factors [15] in SAR imaging which influence the quality of SAR image classification, and obstruct interpretation and applications of SAR images. For land consolidation application, a main restrained factor is the available spatial resolution of SAR images.

The spatial resolution of SAR images includes azimuth resolution and slant range resolution. Azimuth resolution is achieved by combining of many radar returns to simulate a large antenna. The limit to the azimuth resolution of practical spaceborne SAR systems dues to get a reasonable swath width and to avoid a huge amount of data being transmitted to Earth. And slant range resolution is achieved through time-delay measurements using time-dispersed linear frequency modulated pulses which can be compressed into extremely short pulses. The limit to the range resolution comes from the power constraints.

Many earlier works have been done to improve SAR spatial resolution [16, 17]. These works greatly depend on the work mode and hardware set of the imaging radar. And some delightful achievements have been gained. But the resolution can not reach its physical utmost or the optics remote sensing resolution level. Here a key problem is how to process the data from a radar standpoint.

To enhance the resolution beyond the matched filter classical limit, Guglielmi et al. [18] applied super-resolution methods to SAR data. They demonstrated two classes of image reconstruction methods: deterministic regularization and stochastic regularization. Goodman et al. [19, 20] has investigated some stochastic regularization methods for SAR processing of satellite constellations. Some stochastic regularization techniques, such as maximum likelihood estimate and minimum mean-squared error (MMSE) filtering, were introduced, and experiments showed that stochastic regularization techniques can provide better geometric resolution than the traditional matched filtering. But these methods require huge additional computation complexity. An iterative implementation of the minimum mean squared error solution was developed [21]. Although it improved the computation efficiency, it required calculating the inverse for huge matrix repeatedly, thus the complex computation and time consuming were still huge.

To solve the above problems, we develop a new Kalman Filter (KF) scheme integrating the matched filter to obtain high resolution radar image. Traditional Kalman Filter has the limitation of the stringent requirement on precise a priori knowledge of the system models and noise properties, and uncertainty in the covariance parameters of the process noise ($\mathbf{R}_p$) and the observation errors ($\mathbf{R}_o$) may significantly degrade the filtering performance[22, 23]. For the application of land consolidation, the noise levels may change in different spatial zones of the study areas. To scale the noise without artificial or empirical parameters, this paper proposes a new adaptive Kalman Filter process to replace the traditional Kalman Filter algorithm[24, 25, 26]. The most distinct advantage of this proposed scheme is that adaptive Kalman Filter fully utilizes the data to eliminate measurement error due to clutter and to enhance the resolution beyond the matched filter classical limit.

The remainder of this paper is organized as follows. Section 2 develops the mathematical model of SAR land echo signal. Section 3 describes the algorithm of the adaptive Kalman Filter. In Section 4, we report the experimental results and perform some comparisons with traditional methods. Finally, Section 5 concludes this paper.

2 Kalman Filter Model for SAR System

The Kalman Filter (KF) is the most common technique for restoring a signal of interest from other signals, termed noise signals. The Kalman Filter technique formulates a linear discrete system by two stochastic linear recursive equations: the state equation and the measurement equation. For a SAR system, the state equation and the measurement equation of a Kalman filtering can be given as:

$$\begin{aligned}\boldsymbol{\gamma}(i) &= A(i)\boldsymbol{\gamma}(i-1) + \mathbf{n}_p(i) \\ \mathbf{S}_{\mathbf{r}}(i) &= \mathbf{P}(i)\boldsymbol{\gamma}(i) + \mathbf{n}_o(i)\end{aligned} \tag{1}$$

where $\boldsymbol{\gamma}(i)$ is (D×1) state vector, $A(i)$ is (D×D) transition matrix, $\mathbf{S}_{\mathbf{r}}(i)$ is (m×1) observation vector, $\mathbf{P}(i)$ is (m×D) observation matrix, $\mathbf{n}_p(i)$ is the process noise and expresses the uncertainty in the modeling of the expected variation, $\mathbf{n}_o(i)$ represents the measurement errors that occur at each observation time. The noise statistic will satisfy:

$$\begin{aligned}&E\{\mathbf{n}_p(i)\} = E_p, && E[\mathbf{n}_p(i), \mathbf{n}_p(j)] = \mathbf{R}_p\delta_{ij} \\ &E\{\mathbf{n}_o(i)\} = E_o, && E[\mathbf{n}_o(i), \mathbf{n}_o(j)] = \mathbf{R}_o\delta_{ij} \\ &E\{\mathbf{n}_p(i), \mathbf{n}_o(J)\} = 0 &&\end{aligned} \tag{2}$$

where $E\{\bullet\}$ denotes the expectation function. $\mathbf{R}_p$ and $\mathbf{R}_o$ are the covariance matrix of process noise and observation errors, respectively.

Usually it is assumed that there is no range or Doppler walk and that the spaceborne SAR platform is in the far field of the Earth's surface. Therefore, it is reasonable to assume that the state vector comprising of the scattering coefficients keeps approximately constant with respect to time, space, and frequency over the extent of the radar measurement. So the state transition matrix $A(i)$ will be an identity matrix, i.e., $A(i) = \mathbf{I}$ and the state equation of Equation (1) can be rewritten as:

$$\boldsymbol{\gamma}(i) = \boldsymbol{\gamma}(i-1) + \mathbf{n}_p(i) \tag{3}$$

To obtain the measurement equation accurately, now the system signal mode is formulated firstly.

Assuming a radar transmits signal *s(t)*, the signal measured by the radar receiver at time t, due to an unit scatterer located at position $\mathbf{r}$ can be represented as:

$$p(t, \mathbf{r}) = s(t - \tau_{\mathbf{r}}) \tag{4}$$

where $\mathbf{r}$ is the position vector describing surface location of the unit scatterer relative, and $\tau_{\mathbf{r}}$ is the propagation time delay.

From a view point of SAR, time t can be considered as two part: fast time t_f and slow time t_s, and the transmitted signal can be described with fast time t_f. For a common SAR system, the transmitted signal is often chirp scaling signal. Let the chirp rate be k_r, the pulse duration T_r, and the carrier frequency be defined as ω_c, then the transmitted signal is:

$$s_t(t_f) = \exp\left[j\left(\omega_c t_f + k_r t_f^2\right)\right]\mathrm{rect}\left(t_f / T_r\right) \tag{5}$$

where , $\mathrm{rect}(\cdot)$ is defined as:

$$\mathrm{rect}\left(t_f / T_r\right) = \begin{cases} 1 & -T_r/2 \le t_f \le T_r/2 \\ 0 & others \end{cases} \tag{6}$$

During the fast time, the movement of the system can be ignored, thus, the propagation delay $\tau_{\mathbf{r}}$ can be approximated to $\tau_{t_s,\mathbf{r}}$, which only takes the movement in slow time into account. So the signal is:

$$p(t, \mathbf{r}) = p(t_s, t_f, \mathbf{r}) = \exp\left[j\left(-\omega_c \tau_{t_s,\mathbf{r}} + k_f (t_f - \tau_{t_s,\mathbf{r}})^2\right)\right] \cdot \mathrm{rect}\left((t_f - \tau_{t_s,\mathbf{r}}) / T_r\right) \tag{7}$$

The radar geometry is shown in Fig. 1. Assuming a spaceborne SAR system travels at velocity, v_a, and the origin of the coordinate system is located at the system center, the positive x-direction refers to the direction of the system flying direction, z-direction refers to the direction away from the earth surface, and y is given using the right hand rule. Therefore, assuming a flat earth and the altitude of the SAR system is h, the coordinate of dot target on the ground at $t = 0$ is $(x, y, -h)$.So the position vector of the ground target at any given time t can be represented as $\mathbf{r} = (x - v_a t, y, -h)$, and can be simplified as $\mathbf{r} = (x - v_a t, y)$.

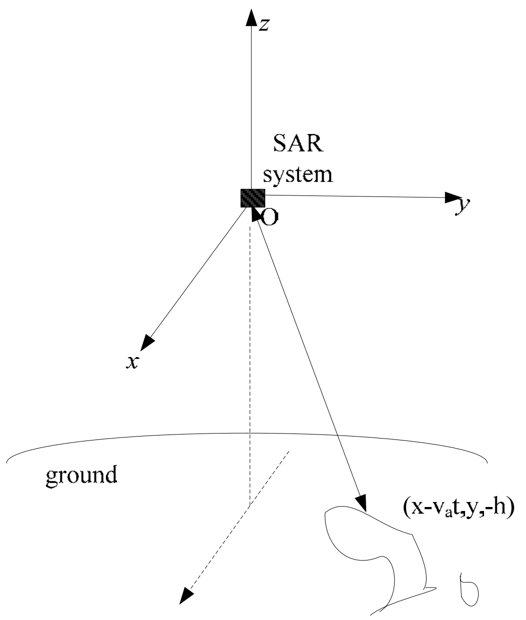

Fig. 1 Radar geometry for Land Consolidation

In terms of the above coordinate system, assuming c the speed of light, the propagation time delay $\tau_{t_s,\mathbf{r}}$ is

$$\tau_{t_s,\mathbf{r}} = \frac{2}{c}\left(\sqrt{(v_a t_s - x)^2 + (y)^2 + (-h)^2}\right) \tag{8}$$

Let the transmitting antenna gain be a constant, the total measurement taken by the receiver due to all illuminated scatterers is:

$$s_r(t) = s_r(t_s, t_f) = \int \gamma(\mathbf{r}) \cdot p(t, \mathbf{r}) d\mathbf{r} + n(t_s, t_f) \tag{9}$$

where $\gamma(\mathbf{r})$ is the back reflectivity at $\mathbf{r}$.

Since the transmitted signal is constrained both in bandwidth and in time, Equation (9) sampled at time t_{sn} and t_{fm} can be approximated with discrete samples as:

$$s_r(t_{sn}, t_{fm}, \mathbf{r}_k) = \sum_i \gamma(A_i) \cdot p(t_{sn}, t_{fm}; A_i)\Delta A + n(t_{sn}, t_{fm}) \tag{10}$$

where $\Delta \mathrm{A}$ refers to unit scatter area, and is a constant, i is the index of different area.

Let

$$\mathbf{S_r} = \left[s_r(t_{s1}, t_{f1}) \cdots s_r(t_{s1}, t_{fN_r}) \quad s_r(t_{s2}, t_{f1}) \cdots s_r(t_{sN_a}, t_{fN_r}) \right]^T \tag{11}$$

$$\boldsymbol{\gamma} = \left[\gamma(A_1) \quad \gamma(A_2) \quad \cdots \quad \gamma(A_D) \right]^T \tag{12}$$

$$\mathbf{P} = \begin{bmatrix} p(t_{s1}, t_{f1}, A_1) & \cdots & p(t_{s1}, t_{f1}, A_2) & \cdots & p(t_{s1}, t_{f1}, A_D) \\ p(t_{s1}, t_{f2}, A_1) & \cdots & p(t_{s1}, t_{f2}, A_2) & \cdots & p(t_{s1}, t_{f2}, A_D) \\ & & \vdots & & \\ p(t_{sN_a}, t_{fN_r}, A_1) \cdots & p(t_{sN_a}, t_{fN_r}, A_2) & \cdots & p(t_{sN_a}, t_{fN_r}, A_D) & \end{bmatrix} \tag{13}$$

$$\mathbf{N} = \left[n(t_{s1}, t_{f1}) \cdots n(t_{s1}, t_{fN_r}) \quad n(t_{s2}, t_{f1}) \cdots n(t_{sN_a}, t_{fN_r}) \right]^T \tag{14}$$

where D is the number of different areas of size $\Delta \mathrm{A}$, sN_a is the sampled number during the slow time interval, fN_r is the sampled number during the fast time interval, and $(\cdot)^T$ denotes the transpose operation.

Then Equation (10) can be represented using matrix-vector notation:

$$\boldsymbol{S_r} = \boldsymbol{P\gamma} + \boldsymbol{N} \tag{15}$$

Equation (15) is the precise express of the measurement equation in Equation (1), so the size of $\mathbf{S_r}(i)$, $m = sN_a \cdot fN_r$. When execute the Kalman Filter based on Equation (15), the data will be divided into I smaller vectors, and i in Equation (1) will be the iteration number or the section of data, varying from 1 to I.

3 Implementation of Adaptive Kalman Filter Algorithm

In a Kalman Filter, all the system characteristics have to be specified a priori as described in section 2. However, if there is uncertainty in any of these characteristics (including initial conditions, and noise characteristics), the filter may not be robust enough. To avoid some of the numeric problems inherent in the standard form of the Kalman Filter, an alternative filter is proposed which performs better than the standard Kalman Filter for uncertainties in both process and measurement noise covariances.

Our adaptive Kalman Filter process includes two main phases: Obtaining the initial parameter by compressing part of the data by the matched filtering to initiate the Kalman filtering process and applying the adaptive Kalman filtering to the rest of the data. This section shows the processing of our developed adaptive Kalman Filter algorithm.

3.1 Initial Parameter Estimate based on Matched Filtering Processing

The selection of the parameters will affect the rate of the convergence. In worse condition, ill-suited initial parameters will make the KF unable to converge at all. Furthermore, if all data are processed with the Kalman Filter, the computational cost will be very large.

To assure the Kalman Filter quality and improve the computation performance, part of the data are selected and compressed with the matched filter firstly in our process scheme. When implementing the adaptive Kalman Filter, we take the result of this phase into account and set the initial state based on the matched filtering result to initiate the filtering process.

How to divide the data up between the matched filter and Kalman Filter? In fact the data can be selected in any manner as long as the matched filtering process limits the number of non-zero pixels to less than the number of measurements available for the Kalman filtering.

Here, we select 1/3 data for the matched filter. A subset of the data is chosen:

$$\mathbf{S}_{\mathbf{r}s} = \left[s_r(t_{s1}, t_{f1}) \cdots s_r(t_{s1}, t_{fN_r}) \cdots s_r(t_{spart}, t_{fN_r}) \right]^T \tag{16}$$

where $spart < sN_a$, here $spart = \mathrm{int}(sN_a / 3)$.

In the same way, a smaller matrix $\mathbf{P}_s$ is gotten from Equation (12) and can be represented as:

$$\mathbf{P}_s = \begin{bmatrix} p(t_{s1}, t_{f1}, A_1) & \cdots & p(t_{s1}, t_{f1}, A_2) & \cdots & p(t_{s1}, t_{f1}, A_D) \\ p(t_{s1}, t_{f2}, A_1) & \cdots & p(t_{s1}, t_{f2}, A_2) & \cdots & p(t_{s1}, t_{f2}, A_D) \\ & & \vdots & & \\ p(t_{sN_a}, t_{fN_r}, A_1) & \cdots & p(t_{sN_a}, t_{fN_r}, A_2) & \cdots & p(t_{sN_a}, t_{fN_r}, A_D) \end{bmatrix} \tag{17}$$

Then the matched filtering can be modeled as the estimation:

$$\hat{\gamma} = \mathbf{W}_{corr} \mathbf{S}_{\mathbf{r}s} \tag{18}$$

where $\mathbf{W}_{corr}$ is the matched filter estimator and $\mathbf{D}_{mf}$ is the diagonal matrix respectively:

$$\mathbf{W}_{corr} = \mathbf{D}_{mf}{}^{-1} \mathbf{P}_{\mathbf{s}}{}^H \tag{19}$$

$$\mathbf{D}_{mf} = \begin{bmatrix} \mathbf{p}_1{}^H \mathbf{p}_1 & 0 & \cdots & 0 \\ 0 & \mathbf{p}_2{}^H \mathbf{p}_2 & \cdots & 0 \\ \vdots & \vdots & \ddots & \vdots \\ 0 & 0 & \cdots \mathbf{p}_s{}^H \mathbf{p}_s & \end{bmatrix} \tag{20}$$

3.2 Adaptive Kalman Filtering Processing

Now it's time to use the adaptive Kalman Filter for the rest of the data to get images with high performance.

The performance of the Kalman Filter relies on the proper definition of the dynamic model and the stochastic model. The stochastic model describes the stochastic properties of the system process noise and observation errors. The process noise ($\mathbf{n}_p$) and the observation errors ($\mathbf{n}_o$) influence the weight that the filter applies between the existing process information and the latest measurements. Any error in them may result in the filter being suboptimal or even cause it to diverge. So the uncertainty in the covariance parameters of $\mathbf{R}_p$ and $\mathbf{R}_o$ has a significant impact on Kalman filtering performance. The conventional way of obtaining the $\mathbf{R}_p$ and $\mathbf{R}_o$ requires good a priori knowledge of the process noise and measurement errors, which typically comes from intensive empirical analysis. In processing, the values are generally fixed and applied during the whole application segment. For the SAR system, the performance suffers from this inflexibility. Because practical process noise and measurement errors are dependent on the application environment and process dynamics. And the settings of the stochastic parameters have to be conservative in order to stabilize the filter for the worst case scenario. This leads to performance degradation.

To reduce the influence of the $\mathbf{n}_p$ and $\mathbf{n}_o$ definition errors and improve the robustness of the adaptive filtering algorithm, the noise statistic is scaled here adaptively.

$$\begin{aligned}
\hat{E}_p(i) &= (1-\frac{1}{i})\hat{E}_p(i-1) + \frac{1}{i}\left[\hat{\boldsymbol{\gamma}}(i) - \hat{\boldsymbol{\gamma}}(i-1)\right] \\
\hat{\mathbf{R}}_p(i) &= (1-\frac{1}{i})\hat{\mathbf{R}}_p(i-1) + \frac{1}{i}\left[\mathbf{K}(i)\mathbf{w}(i)\mathbf{w}(i)^T\mathbf{K}(i)^T + \hat{\mathbf{K}}_{\mathbf{g}}(i) - \hat{\mathbf{K}}_{\mathbf{g}}(i-1)\right] \\
\hat{E}_0(i) &= (1-\frac{1}{i})\hat{E}_o(i-1) + \frac{1}{i}\left[\mathbf{S}_{\mathbf{r}}(i) - \mathbf{P}(i)\tilde{\boldsymbol{\gamma}}(i)\right] \\
\hat{\mathbf{R}}_o(i) &= (1-\frac{1}{i})\hat{\mathbf{R}}_o(i-1) + \frac{1}{i}\left[\mathbf{w}(i)\mathbf{w}(i)^T - \mathbf{P}(i)\tilde{\mathbf{K}}_{\mathbf{g}}(i)\mathbf{P}(i)^T\right]
\end{aligned} \tag{21}$$

So the adaptive Kalman Filter is:

$$\hat{\boldsymbol{\gamma}}(i) = \tilde{\boldsymbol{\gamma}}(i) + \mathbf{K}(i)\mathbf{w}(i) \tag{22}$$

where $\mathbf{w}(i)$ is termed as the innovation and $\mathbf{K}(i)$ is the Kalman gain matrix, they are expressed as follows:

$$\begin{aligned}
\mathbf{w}(i) &= \mathbf{S}_{\mathbf{r}}(i) - \mathbf{P}(i)\tilde{\boldsymbol{\gamma}}(i) - \hat{E}_0(i-1) \\
\mathbf{K}(i) &= \tilde{\mathbf{K}}_{\mathbf{g}}(i)\mathbf{P}(i)^T\left(\mathbf{P}(i)\tilde{\mathbf{K}}_{\mathbf{g}}(i)\mathbf{P}(i)^T + \hat{\mathbf{R}}_o(i-1)\right)^{-1} \\
\tilde{\boldsymbol{\gamma}}(i) &= \hat{\boldsymbol{\gamma}}(i) + \hat{E}_p(i-1) \\
\tilde{\mathbf{K}}_{\mathbf{g}}(i) &= \hat{\mathbf{K}}_{\mathbf{g}}(i-1) + \hat{\mathbf{R}}_p(i-1) \\
\hat{\mathbf{K}}_{\mathbf{g}}(i) &= \left(\mathbf{I} - \mathbf{K}(i)\mathbf{P}(i)\right)\tilde{\mathbf{K}}_{\mathbf{g}}(i)
\end{aligned} \tag{23}$$

The steps are repeated until all the radar measurements are used, and then the estimation is the result. The initial $\hat{\boldsymbol{\gamma}}(0)$, $\tilde{\mathbf{K}}_{\mathbf{g}}(0)$ have to be set to initiate the filtering process. The initial $\hat{\boldsymbol{\gamma}}(0)$ will be set as the result of the filtering in the matched filtering. The initial $\tilde{\mathbf{K}}_{\mathbf{g}}(0)$ is computed based on the results of the matched filtering and Equation (23).

4 Experimental Results

Presented experimental results are aimed at showing the performance of the proposed filtering algorithm with respective to four aspects: 1) the spatial resolution, 2) the error criterion, 3) the computing speed, and 4) the converge rate. To demonstrate the resolution performance straightly, in this section, a simulated scene with 5 uniformly spaced dots placed on the earth surface is considered, and the raw data sets have been generated using the signal model mentioned before.

Images in Fig. 2 show the filtering results obtained by the matched filter, the MMSE filter, the traditional Kalman Filter and the adaptive Kalman Filter respectively for various SNRs. The SNRs are: low SNR (-20dB), moderate SNR (0dB) and high SNR (20dB). It can be seen that for all the SNR scenarios considered, Kalman Filter gives better estimates than the matched filter in terms of resolution performance. Especially in the high SNR situation, Kalman Filter minimizes correlation with other pixels in order to reduce the error due to clutter, but the matched filter is seen to be clutter limited. Even though the matched filter estimate of the scattering coefficients improves with SNR, it is still unable to describe the image of a dot object with an area less than 5 pixels in any case. In the low-SNR case, the adaptive Kalman Filter scales the filter to rely on target statistics and outperforms the traditional Kalman Filter result. The results also prove that the matched filter is optimal in the sense of the output signal-to-noise ratio.

It also demonstrates that the traditional Kalman Filter gives the same estimate as given by MMSE, which validates that the Kalman Filter is an iterative form of the MMSE filter.

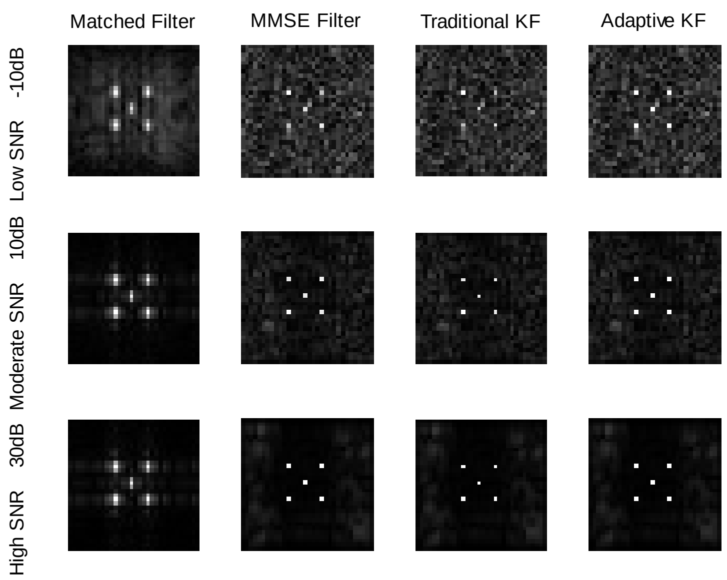

Fig. 2 Comparison of the Matched filter, the MMSE Filter , the traditional Kalman Filter and the adaptive Kalman Filter performance versus SNR

To assess performance of different algorithms numerically, simulation results in terms of the error criterion will be taken into account. The error criterion is the mean-squared error (MSE) of the pixel magnitudes normalized by the image's mean-squared pixel magnitude:

$$MSE = \frac{(\hat{\gamma}-\gamma)^H (\hat{\gamma}-\gamma)}{\gamma^H \gamma} \tag{24}$$

Fig. 3 shows the variation of the Normalized MSE as a function of input SNR. It shows that the adaptive Kalman Filter has the lowest error at both low SNR and high SNR. But at moderate SNR, the MSE of the adaptive Kalman Filter is higher because the using of matched filtering for part data. For land consolidation application, the SNR is usually about 20dB, so the adaptive Kalman Filter will bring less error to images.

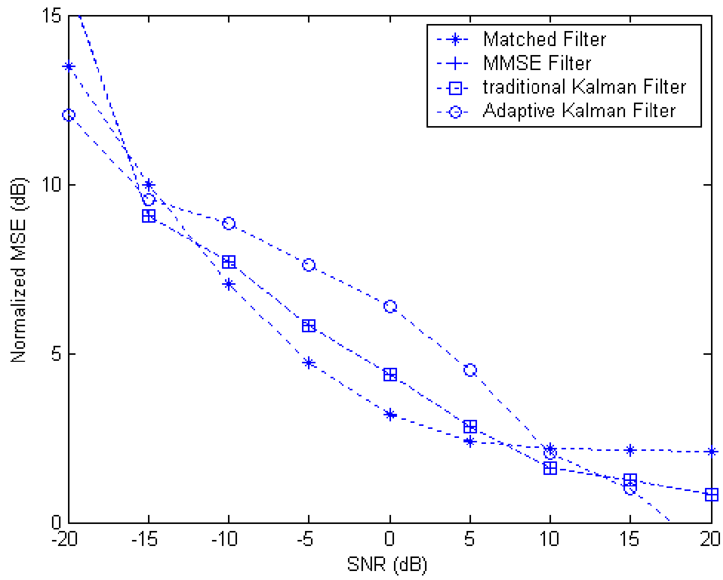

Fig. 3 MSE performance of the Matched filter, MMSE filter, the traditional Kalman Filter and the adaptive filter versus SNR

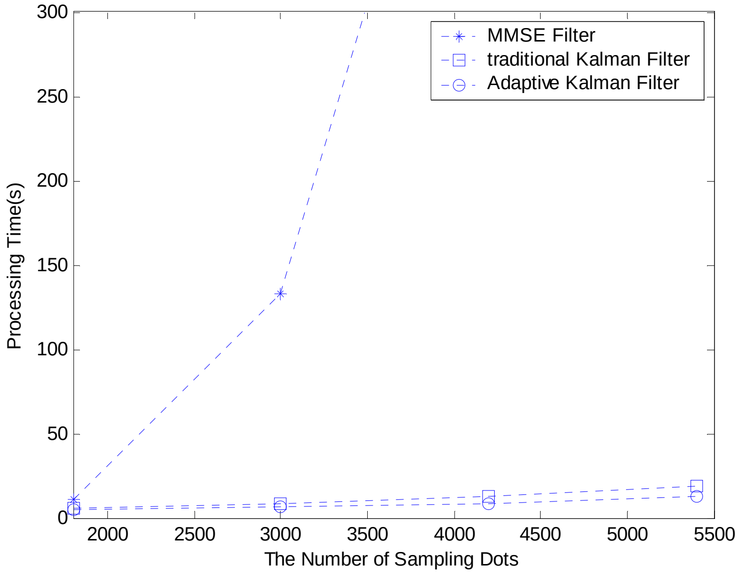

Fig. 4 Processing speed of the Matched filter, MMSE filter, the traditional Kalman Filter and the adaptive Kalman Filter

Another important advantage of the developed algorithm is its ability of decreasing the processing load inherent in the MMSE filter and the traditional KF. Fig. 4 shows this improvement obtained. The processing time for different number of sampling dots is shown. The processing is done in Matlab on a PC with 512M RAM and a 2.93 GHz processor. It can be seen that as the number of radar measurements increases, the processing time for MMSE increases huge fold. But in the case of the KF, there is only a slight change in the processing time. Most important, the adaptive KF takes about half of processing time of the traditional KF, especially when the number of sampling measurements is increased. The results validate the developed adaptive KF.

To validate the converge rate of the adaptive KF, the improvement in the estimation of a unit dot scattering versus the iteration times can be viewed in the images given in Fig. 5. The iteration times are indicated at the top of each image.

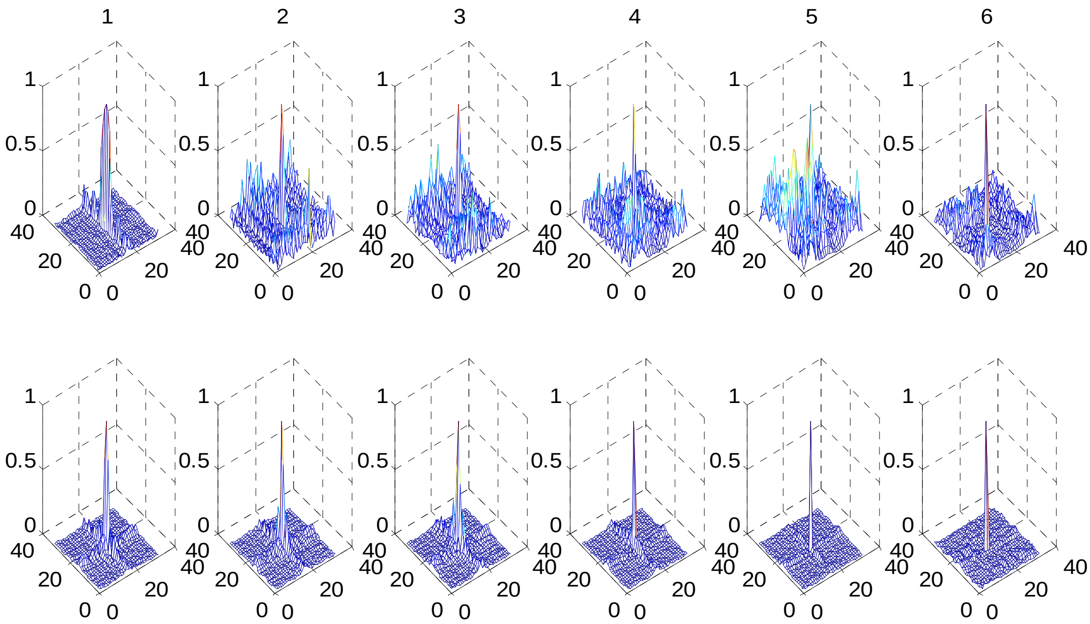

Fig. 5 KF estimation obtained for each iteration

It can be seen from Fig. 5 that there is a lot of improvement along with the iteration. For the traditional KF the initial value of $\hat{\gamma}(0)$ is set to be zeros , $\tilde{\mathbf{K}}_{\mathbf{g}}(0)$ is set according to the SNR. So in the early stages the traditional KF mainly reduce the interference between the targets present in the radar measurement, and to get better estimation, it need more iteration times. Howbeit, the adaptive KF gets good estimation more quickly. The result testifies the efficiency of the developed adaptive KF.

5 Conclusion

SAR system enables to obtain all day/all night and all weather information for land consolidation. But land consolidation application requires high resolution images. To obtain high resolution SAR images, a signal space representation of the radar was presented and facilitated the discussion of reconstruction filter algorithms. The developed adaptive Kalman Filter procedure was applied to the simulated radar data. Results were also presented and demonstrated the feasibility of the high resolution SAR. A summary of the advantage of our algorithm is given as follows.

1) The traditional matched filter was combined with the Kalman Filter, which improves the computing speed as well as the performance of the estimate.
2) The noise statistic in the Kalman Filter model is scaled adaptively. So the influence of the noise definition errors is reduced and the robustness of the adaptive filtering algorithm is improved.

In future, further tests will be performed by using real measured data on spaceborne SAR platform.

Acknowledgement

This work has been supported by The National High Technology Research and Development Program of China (Project contract number: 2006AA12Z129).

The authors express gratitude to the domain experts from Land Consolidation Centre, The Ministry of Land and Resources P.R.C, Beijing Oriental TITAN Technology Co. LTD, EU-China Center for Information & Communication Technologies of China Agricultural University, for their constant support.

References:

[1] Monke, E., Avillez, F., Ferro, M., Consolidation policies and small-farm agriculture in Northwest Portugal. *European Review of Agricultural Economics*, 1992, Vol. 19, pp. 67–83.

[2] Terry, v. D., Complications for traditional land consolidation in Central Europe, *Geoforum*, Vol. 38, No. 3, 2007, pp. 505-511.

[3] Huang, J., Wang, R., Zhang, H., Land consolidation and GIS application in Xinjiang, China, *Proceedings of the SPIE*, Vol. 6411, 2006, pp. 64111S .

[4] Liu, M., Wu, Z., Davis, J., Land consolidation and productivity in Chinese household crop production, *China Economic Review*, 2005, Vol. 16, pp. 28–49.

[5] Gopal, B. T., Gajendra, S. N., Alternative options of land consolidation in the mountains of Nepal: An analysis based on stakeholders' opinions, *Land Use Policy*, Vol. 25, No. 3, 2008, pp. 338-350.

[6] Sevkiye, S. T., An analysis on the efficient applicability of the land readjustment (LR) method in Turkey, *Habitat International*, Vol. 31, No. 1, 2007, pp. 53-64.

[7] Hwang, D. Y., Wu, W. H., Financial system reform in Taiwanb, *Journal of Asian Economics*, Vol. 18, No. 1, 2007, pp. 21-41.

[8] Petr, S., Applying evaluation criteria for the land consolidation effect to three contrasting study areas in the Czech Republic, *Land Use Policy*, Vol. 23,No. 4, 2006, pp. 502-510.

[9] Pietro, T., Luigi, T., Tazio, S., Laura, C., Urs, W., Federica, R., Mapping regional land displacements in the Venice coastland by an integra ted monitoring system, *Remote Sensing of Environment*, Vol. 98, No. 4, 2005, pp. 403-413.

[10] Mario, G., Priska, B., Brett, H. R., Peter, B., Combining classification tree analyses with interviews to study why sub-alpine grasslands sometimes revert to forest: A case study from the Swiss Alps, *Agricultural Systems*, Vol. 96, No. 1-3, 2008, pp. 124-138.

[11] Cay, T., Corumluoglu, O., Iscan, F., A study on productivity of satellite images in the phanning phase of land consolidataion projects, *Proceedings of ISPRS2004*, 2004, pp. 379-385.

[12] Vallone, P., Giammarinaro, M.S., Crosetto, M., Agudo, M., Biescas, E., Ground motion phenomena in Caltanissetta (Italy) investigated by InSAR and geological data integration, *Engineering Geology*, Vol. 98, No. 3-4, 2008, pp. 144-155.

[13] Martin, G., Werner, A., Christian, M., Gerd, T., Classification of sediments on exposed tidal flats in the German Bight using multi-frequency radar data, *Remote Sensing of Environment*, Vol. 112,

No. 4, 2008, pp. 1603-1613.

[14] Bruno, D., Hobbs, S. E., Ottavianelli, G., Geosynchronous synthetic aperture radar: Concept design, properties and possible applications, *Acta Astronautica*, Vol. 59, No. 1-5, 2006, pp. 149-156.

[15] Huang, S. Q., Liu, D. Z., Some uncertain factor analysis and improvement in spaceborne synthetic aperture radar imaging, *Signal Processing*, Vol.87, No.12, 2007, pp. 3202-3217.

[16] Munson, D.C., O'Brien, Jr. , Jenkins, W. K., A tomographic formulation of spotlight-mode synthetic aperture radar, *Processing of the IEEE*, Vol.72, No.8, 1983, pp. 917-925.

[17] Prati, C., Rocca, F., Improving slant-range resolution with multiple SAR surveys, *IEEE Transaction on Aerospace and Electronic Systems*, Vol.29, No.1, 1993, pp. 135-143.

[18] Guglielmi, V., Castanie, F., Piau, P. , Application of super-resolution methods to synthetic aperture radar data, *Geoscience and Remote Sensing Symposium, IGARSS '95*, 1995, pp. 2289-2291.

[19] Goodman, N., Stiles, J., Resolution and Synthetic Aperture characterization of sparse radar arrays, *IEEE Transaction on Aerospace and Electronics Systems*, Vol. 39, No. 3, 2003, pp. 921-934.

[20] Goodman, N., *SAR and MTI* processing *of sparse satellite clusters*, Doctoral thesis, The University of Kansas, July 2002.

[21] Gullapalli, S., *Application of Kalman Filtering Technique for SAR Processing of Sparse Satellite Clusters*, Master's Thesis, The University of Kansas, December 2002.

[22] Jwo, D. J., Cho, T. S., A practical note on evaluating Kalman filter performance optimality and degradation, *Applied Mathematics and Computation*, Vol. 193, No. 2, 2007, pp. 482-505.

[23] Zhu, X., Soh, Y. C., Xie, L. H., Design and analysis of discrete-time robust Kalman filters, *Automatica*, Vol. 38, No. 6, 2002, pp. 1069-1077.

[24] Weng, S. K., Kuo, C. M., Tu, S. K., Video object tracking using adaptive Kalman filter, *Journal of Visual Communication and Image Representation*, Vol. 17, No. 6, 2006, pp. 1190-1208.

[25] Vincenzo, L., Bruno, S., Luigi Villani Adaptive extended Kalman filtering for visual motion estimation of 3D objects, *Control Engineering Practice*, Vol. 15, No. 1, 2007, pp. 123-134.

[26] Liang, Y., An, D. X. Zhou, D. H., Pan, Q., A finite-horizon adaptive Kalman filter for linear systems with unknown disturbances, *Signal Processing*, Vol. 84, No. 11, 2004, pp. 2175-2194.